Supporting Information

Gravure Printing for Mesoporous Film Preparation

*Nicole Herzog, Robert Brilmayer, Mathias Stanzel, Anastasia Kalyta, Dieter Spiehl, Edgar Doersam, Christian Hess and Annette Andrieu-Brunsen**

Characterization of gravure printed mesoporous silica:

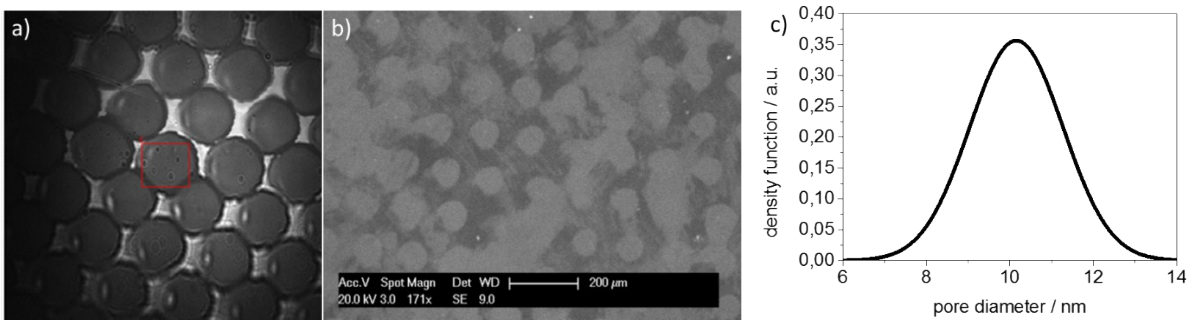

Figure S1. a) Image (5X magnification) of a film printed with F127 ink (6-8 nm pore diameter) at 500 N and a printing cylinder cell depth of 0.45 mL m^{-2}. b) SEM micrograph showing the printed pattern of the same film. Because of the small cell volume and thus the low amount of transferred sol, the ink has not completely covered the substrate before solvent evaporation and silica film formation. A relatively high refractive index (1.872) indicates that this film may not be mesoporous. c) Corresponding pore size distribution to 8-16 nm pores (10.2 ± 1.2 nm).

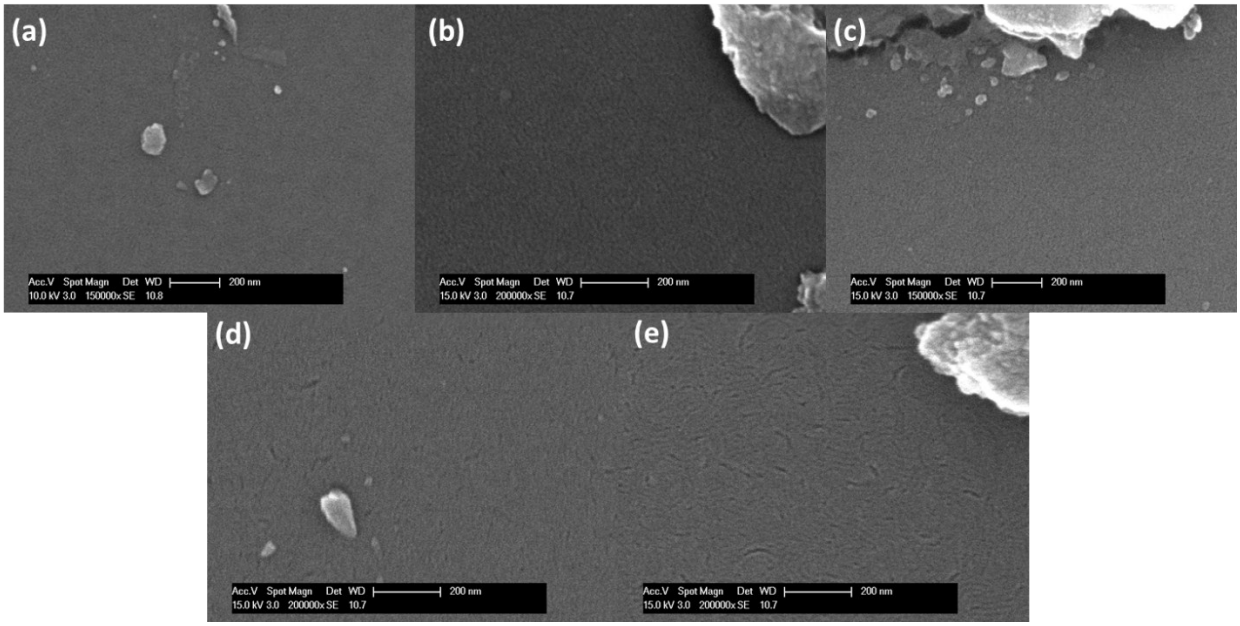

Figure S2. SEM micrographs showing the defect-free homogeneous film structure of various films printed on silicon wafer: (a) unmodified mesoporous silica printed with a 8.5 mL/m^2 cylinder, (b) co-condensed with a 5 mol% (Bis(2-hydroxyethyl)-3-aminopropyl-triethoxysilane), 8.5 $mL\,m^{-2}$ cylinder, (c) 10 mol%(Bis(2-hydroxyethyl)-3-aminopropyl-triethoxysilane), 8.5 $mL\,m^{-2}$ cylinder, (d) 15 mol% coinitiator with 8.5 $mL\,m^{-2}$ cylinder, (e)

20 mol% (Bis(2-hydroxyethyl)-3-aminopropyl-triethoxysilane), 8.5 $mL\,m^{-2}$ cylinder. Measurements taken after sputtering samples with a 3 nm platinum-palladium layer.

Characterization of pore size distribution

The TEM imaged is scaled using ImageJ developed by Wayne Rasband. 20 independent pores were manually measured. The average and standard deviation was calculated. For the graphical evaluation the density function of the normal distribution was used.

$$f(x) = \frac{1}{\sqrt{2\pi\sigma^2}} exp\left\{\frac{(x-\mu)^2}{2\sigma^2}\right\}$$

μ = expected value (average of pore size in nm)

σ = standard deviation

Further ellipsometry and IR characterization of dip-coated and gravure printed mesoporous silica films:

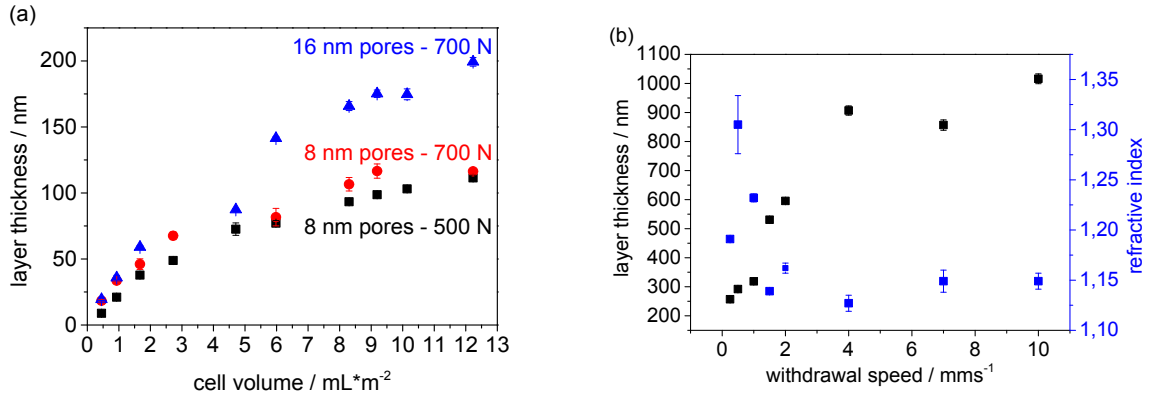

Figure S3. a) Film thickness, as measured by ellipsometry for mesoporous silica films in dependence of the used printing force and the applied ink, giving different pore size of 8 nm and 16 nm, gravure printed with different cell volume. The porosity of the mesoporous silica films is between 40 and 50 % besides low cylinder volume. b) Film thickness and refractive index measured by ellipsometry for mesoporous silica with 16 nm pore size in dependence of withdrawal speed of the dip-coating process. The withdrawal speed depended layer thickness is analogue to results published by Faustini *et al.*.[1]

Besides, ATR-IR can even be used to indirectly determine mesoporous film thickness, after normalizing all spectra to the Si-OH stretching vibration at 970 cm^{-1}. For mesoporous silica films with film thicknesses larger than ~300 nm the asymmetric Si-O-Si stretching vibration at 1060 cm^{-1} is detected. Simultaneously an increase of the Si-O-Si symmetric stretching vibration at around 770 cm^{-1} with increasing film thickness is observed. This effect originates from the well-defined penetration depth of the ATR-IR evanescent field of approximately one micrometer which thus not only detects the mesoporous silica film but as well parts of the supporting glass substrate (Figure S4). With increasing mesoporous silica film thickness the detected ratio between glass substrate and mesoporous silica film and thus the ratio between Si-O-Si stretching vibration at 1060 cm^{-1} and Si-O-Si symmetric stretching vibration at around 770 cm-1 changes proportionally. After scratching the calcinated (350 °C) mesoporous film off the supporting substrate no influence of film thickness on the detected ATR-IR spectra is observed anymore. Consequently, the observed film thickness dependent difference in ATR-IR spectra recorded on substrate supported mesoporous silica films with respect to the symmetrical (800-820 cm^{-1}) and asymmetrical (1000-1260 cm^{-1}) Si-O-Si stretching vibration and silanol vibrational band (900-980 cm^{-1}) (Figure S4) can be clearly attributed to the detected mesoporous film thickness dependent ratio of detected glass substrate to mesoporous film.

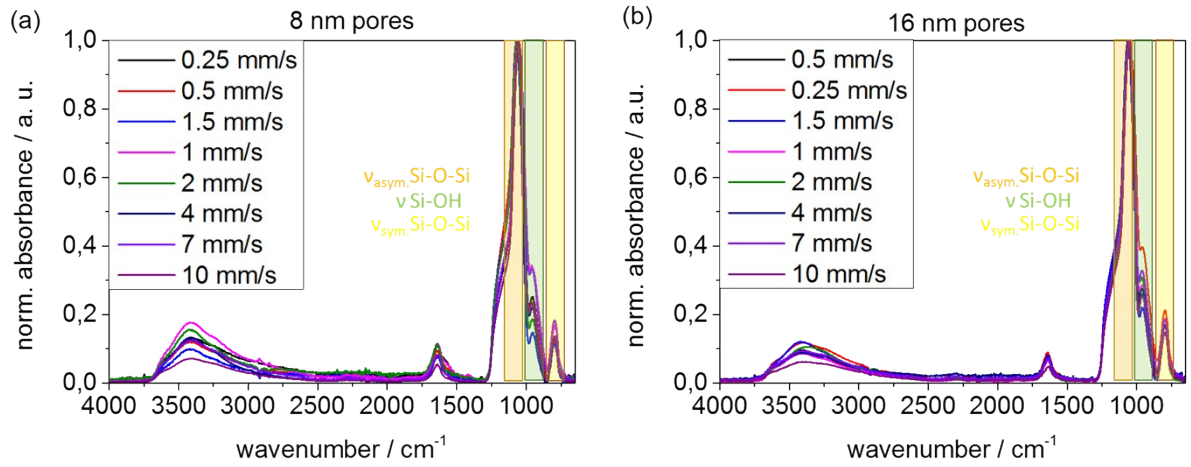

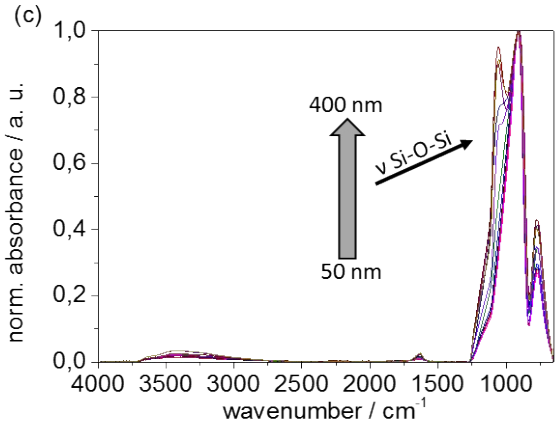

Figure S4. ATR-IR-measurements of scratched mesoporous silica films prepared via dip-coating and template calcination for both pore sizes 8 nm (a) and 16 nm (b). (c) Infrared spectra of the mesoporous film in dependence of the dip-coating withdrawal speed after template calcination at 350°C measured directly on a glass substrate.

Cyclic voltammetry of ITO coated glass as reference:

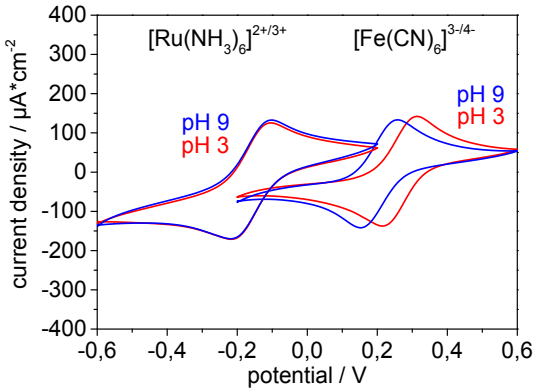

Figure S5. Cyclic voltammetry measurements of an untreated indium-tin-oxid electrode at a scanrate of 100 mV s^{-1} and a pH 3 (red) and pH 9 (blue) using $[Ru(NH_3)_6]^{2+/3+}$ and $[Fe(CN)_6]^{3-/4-}$ as an ionic redox probe molecule at a concentration of 0.01 mM in 100 mM KCl as comparison to Figure 3.

Use of Randles-Sevcik-Equation of cyclic voltammetry measurements (Figure 3):

The squareroot of the scanrate ($\nu^{1/2}$) in dependence of the peak currents ($I_{red/ox}$). A linear increase obeying the Randles-Ševcik equation is observed. With the Randles-Ševcik equation, the slope of the line can be used to determine the diffusion coefficient (D). The other sizes are known.

$$I_P = (2{,}69 \cdot 10^5) \cdot n^{\frac{3}{2}} \cdot A \cdot D^{\frac{1}{2}} \cdot c_i \cdot \nu^{\frac{1}{2}}$$

I_P = current peak for oxidation or reduction [A]
n = number of unreacted electron per molecule
A = surface of the electrode [m^2]
D = diffusion constant [m^2 s^{-1}]
c_i = concentration of redox-active molecule [mol L]

ν = scanrate [V s^{-1}]

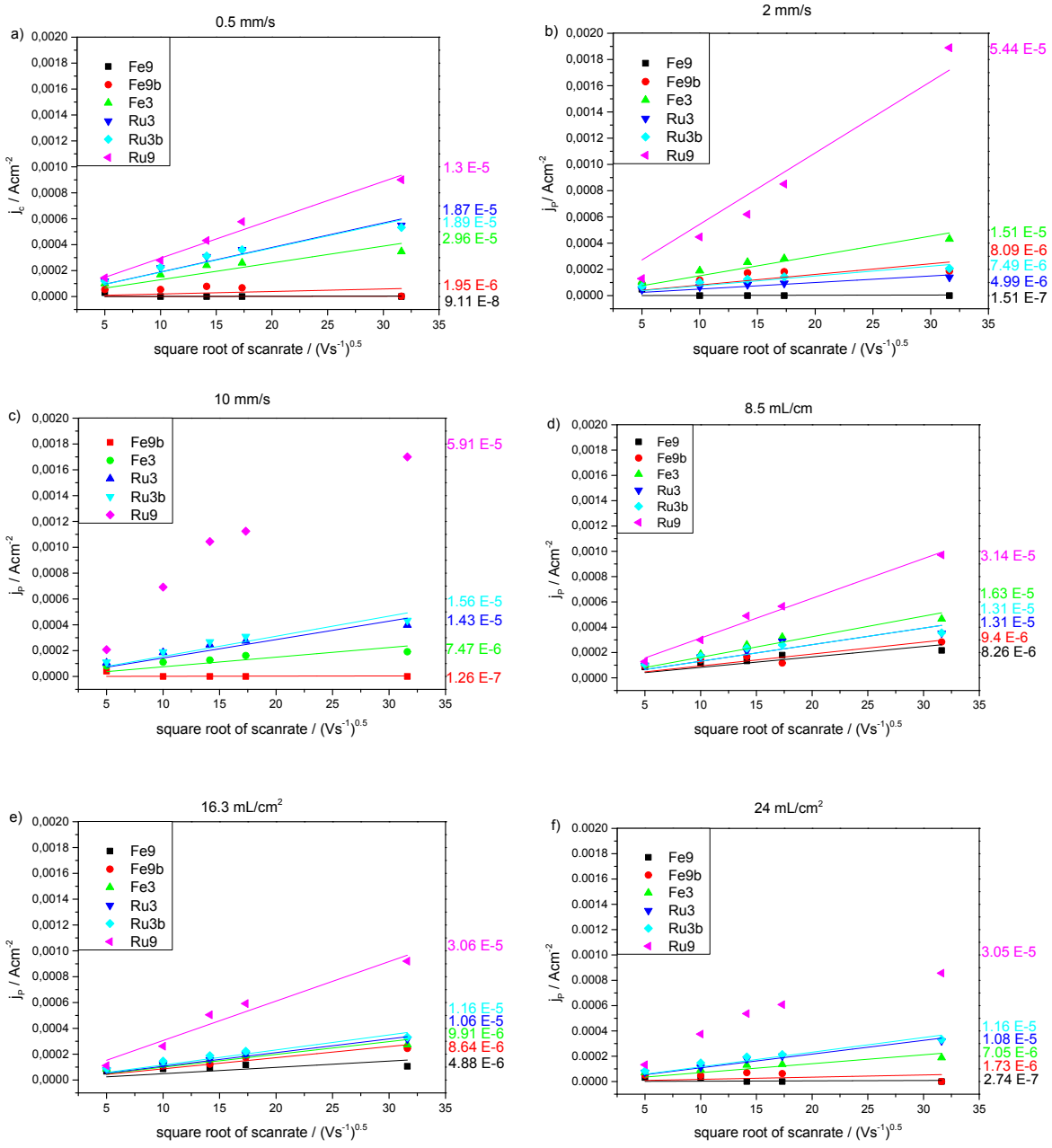

Figure S6. Randles-Sevcik relation with Ip extracted from cyclic voltamograms of mesoporous silica thin films using $[Ru(NH_3)_6]^{2+/3+}$ (-0.6 V - + 0.2 V) (Ru) and $[Fe(CN)_6]^{3-/4-}$ (-0.2 V - +0.6 V) (Fe) as ionic redox probes at pH 3 and 9. The dip-coated mesoporous silica films are prepared with different withdrawal speeds a) 0.5 mm s^{-1} b) 2 mm s^{-1} and c) 10 mm s^{-1} resulting in film thicknesses of a) 140 nm (47 vol% porosity), b) 180 nm (44 vol% porosity), c) 300 nm (39 vol% porosity). Mesoporous silica films prepared by gravure printing are prepared using different cell volumes of d) 8.5 mL m^{-2} e) 16.3 mL m^{-2} and f) 24 mL m^{-2} resulting in film thicknesses of d) 100 nm (48 vol% porosity), e) 162 nm (40 vol% porosity), f) 250 nm (48 vol% porosity). The data sports were fitted with a linear fit and the resulting slope is written in the same color next to the graphs. For c) and f) for basic pH and the positive probe molecule no linear fitting is possible.

Influence of calcination temperature on perm selectivity of mesoporous silica films

Specifically, the effect of template calcination at 350 °C on pH-dependent mesoporous film ionic permseletivity for dip-coated mesoporous films with pore sizes of 8 nm and 16 nm as compared to a maximum temperature treatment limited to 200 °C followed by chemical template extraction using acidic ethanol is shown in **Figure 4**. In accordance to ATR-IR data (SI, Figure S5) which show higher silica condensation degrees and thus less accessible surface Si-OH groups at the mesopore walls (Si-OH vibrational band at 980 cm^{-1}) the observed j_p for $[Ru(NH_3)_6]^{2+/3+}$ decrease with increasing temperature. Furthermore, for both mesopore sizes of 8 nm and 16 nm heating only up to 200 °C and subsequent chemical extraction leads to a more pronounced pH-induced change of ionic permselectivity of ~ 100 µA/cm² as compared to films treated up to 350 °C (~ 80 µA/cm²) indicating a higher concentration of pH-sensitive silanol groups for films treated only up to 200 °C (**Figure 4**). In addition, the pH dependent j_p values for negative charged molecule $[Fe(CN)_6]^{3-/4-}$ show two discontinuous steps which are well visible for both mesoporous films independent on pore diameter or condensation degree. This effect indicates the presence of different types of silanol groups, as reported in literature with two explanations: On the one hand as out-of-plane silanols and in-plane silanols and on the other hand with the existents of Q^2 and Q^3 group silanols.[2, 3] Both theories resulting in two pK_a-values. Unfortunately, determination of the first pK_a value would need j_p values for even more acidic pH values which is not possible due to of the limited stability of mesoporous silica films. A second pK_a value of around 6 for 16 nm pore diameter films and around 7.5 for 8 nm pore diameter films treated up to 350 °C determined from the j_p titration curves of $[Fe(CN)_6]^{3-/4-}$, as well indicating an effect of pore size and thus of spatial confinement. The absolute values differ from pK_a given by literature with 5.6 and 8.5 for silica, which supports as well the presence of confinement controlled pK_a shift in these mesopores.[2]

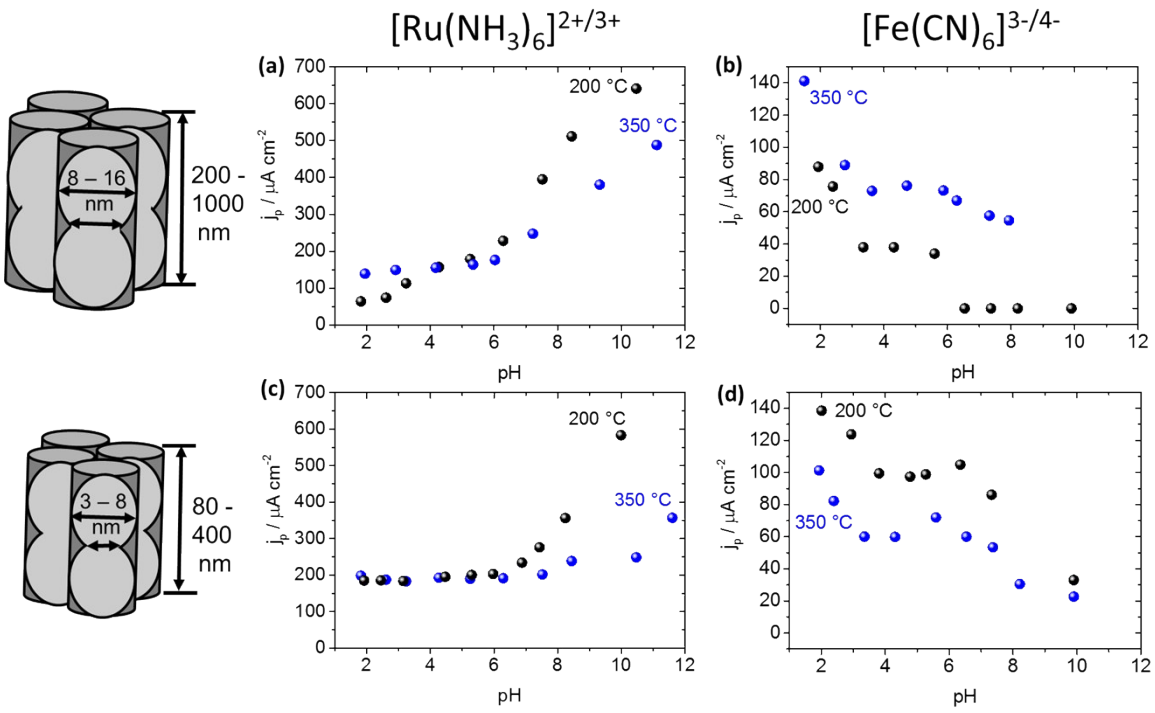

Figure S7. Cyclic voltammetry measurements for positively charged probe molecule $[Ru(NH_3)_6]^{2+/3+}$ (a, c) and the negative charged probe molecule $[Fe(CN)_6]^{3-/4-}$ (b, d) for two different pore sizes big pores of 8-16 nm and small pores of 3-8 nm. The film thickness is as well different with 170 nm in the case of 3-8 nm pores and 350 nm in case of 8-16 nm pores. The black dots represent mesoporous silica films treated up to 200 °C followed by chemical template extraction. Blue dots represent mesoporous silica films calcined till 350 °C. The current density j_P is applied by using different pH-values between 1 and 12.

I_p and porosity in dependence of film thickness:

IR characterization in terms of condensation degree of mesoporous silica with different thermal treatment:

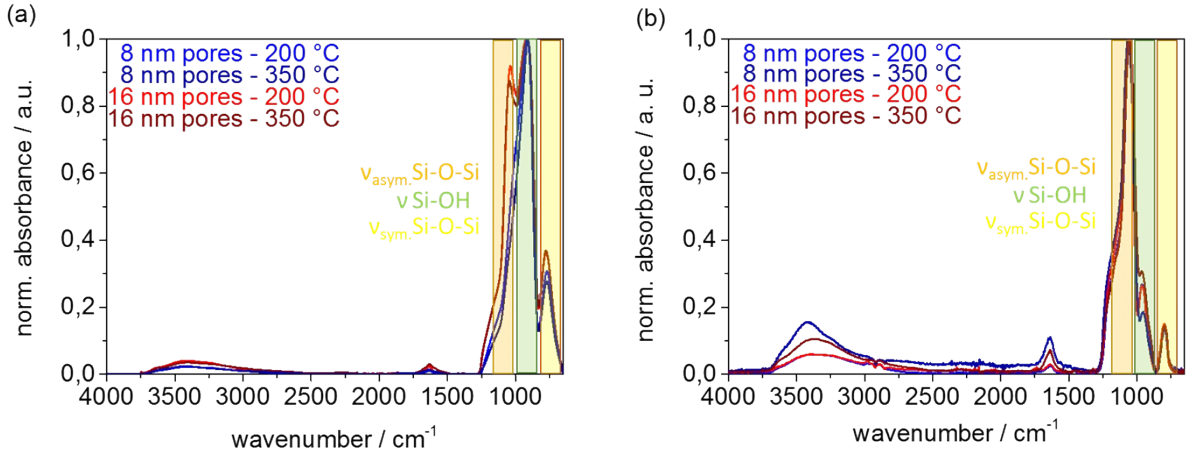

Figure S8. ATR-IR-measurements of mesoporous silica films after template calcination (350 °C) or after temperature consolidation up to 200°C followed by chemical template extraction. a) ATR-IR measured directly on the glass substrate for both pore sizes 8 nm and 16 nm. The spectra show that no template is left in the mesoporous silica films. No CH/ CH_2/CH_3 vibrational bands between 2750 and 3000 cm^{-1} are visible. b) ATR-IR measurements of mesoporous silica films after being scratched off the substrate. The silanol vibration at 950

cm^{-1} is higher for the template extracted mesoporous silica films than for the fully calcinated mesoporous silica films being consistent with a lower condensation degree at lower temperatures.

Comparison of co-condensed mesoporous silica and post grafted mesoporous silica:

The difference between co-condensation and post grafting of (Bis(2-hydroxyethyl)-3-aminopropyl-triethoxysilane) is visible by characterization of the corresponding macroscopic static contact angles (Figure S7). The change of contact angle after post-grafting is much more pronounced than using co-condensation. This indicates a higher functional density after post-grafting, as expected. These results are supported by the cyclic voltammetry measurements shown in Figure S9 considering the (Bis(2-hydroxyethyl)-3-aminopropyl-triethoxysilane) K_a value of 8.7. The influence of the positive charge on mesoporous silica wall can be shown in cyclic voltammetry resulting into an exclusion of positively charged $[Ru(NH_3)_6]^{2+/3+}$ at pH 3 for the post grafted mesoporous silica films. After co-condensation only a decreasing peak current I_p but no exclusion of positively charged ions is observed.

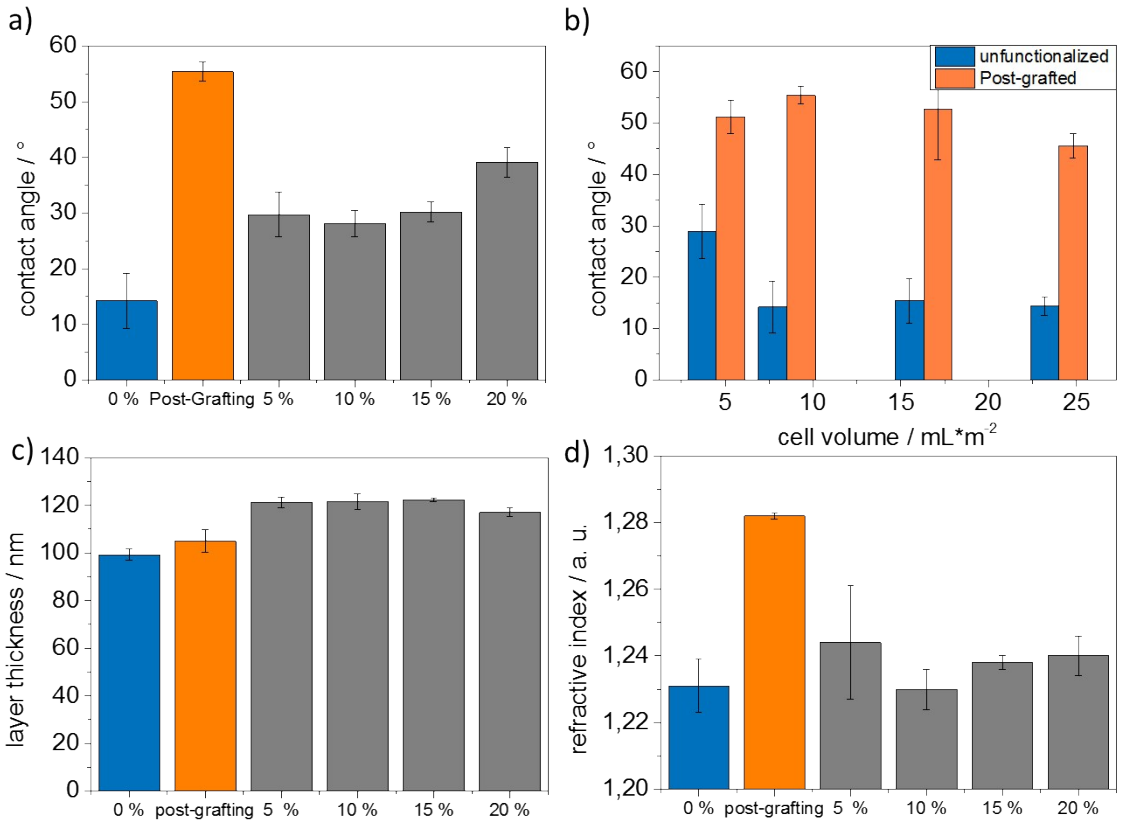

Figure S9. Comparing the functionalization of gravure printed mesoporous silica films with silane (Bis(2-hydroxyethyl)-3-aminopropyl-triethoxysilane) via post-grafting or co-condensation. a) Macroscopic static contact angle measurements with 2 µL water drops for mesoporous silica films with different co-condensation degree b) Macroscopic static contact angles measurements of mesoporous films prepared with different printing cylinder cell volumes with and without (Bis(2-hydroxyethyl)-3-aminopropyl-triethoxysilane) functionalization. Film thickness c) and refractive index d) obtained via ellipsometry for different co-condensation degrees and postgrafting of mesoporous silica prepared with a printing cylinder cell volume of 8 mL m^{-2} via gravure printing.

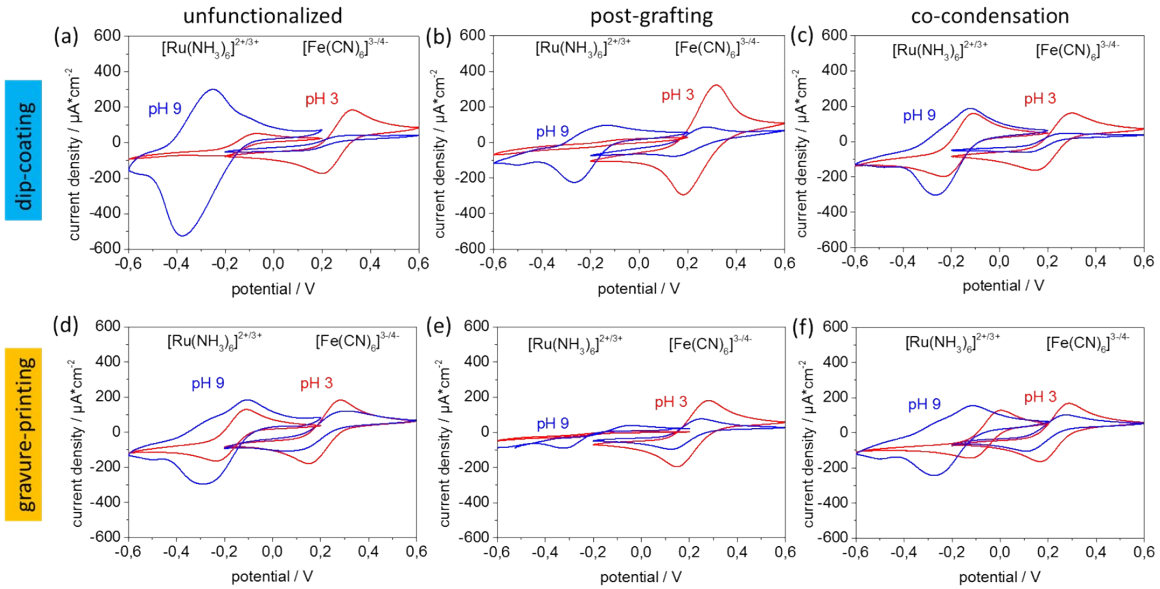

Figure S10. Effect of (Bis(2-hydroxyethyl)-3-aminopropyl-triethoxysilane) functionalization on mesoporous silica film permselectivity prepared via dip-coating with 2 mm s^{-1} withdrawal speed (a-c) resulting in 180 nm film and prepared via gravure printing with 8.5 mL m^{-2} cell volume (d-f) resulting in 100 nm film as obtained by cyclic voltammetry using $[Ru(NH_3)_6]^{2+/3+}$ and $[Fe(CN)_6]^{3-/4-}$ as an ionic redox probes at pH 3 (red) and 9 (blue). a) and d) show the unmodified mesoporous silica films b) and e) the mesoporous silica films after (Bis(2-hydroxyethyl)-3-aminopropyl-triethoxysilane) post grafting in toluene at 80 °C c) and f) the mesoporous silica films with 5 mol % co-condensed (Bis(2-hydroxyethyl)-3-aminopropyl-triethoxysilane) as in-situ functionalization.

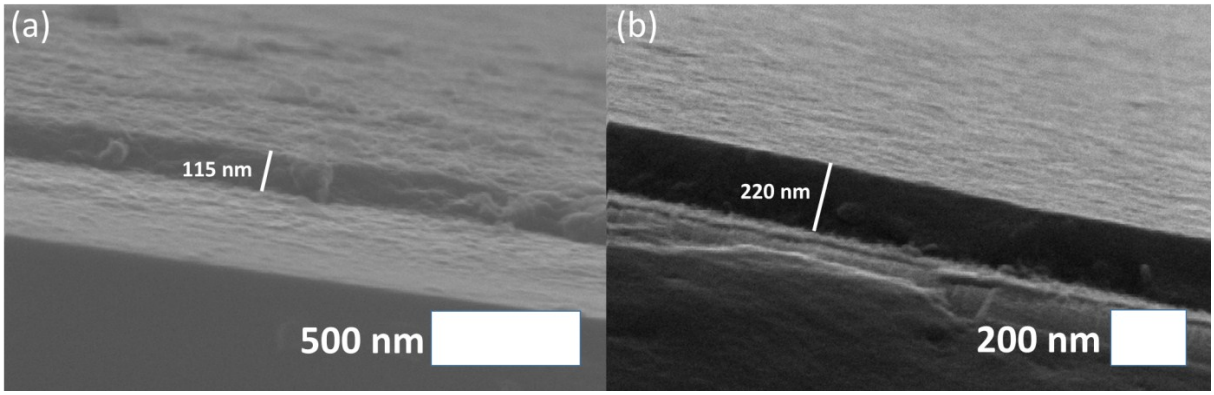

Figure S 11. Cross-section SEM image of a gravure printed mesoporous silica film using the gravure cylinder cell volumes 8.5 mL/m² for printing. a) one layer of 5 mol % of (Bis(2-hydroxyethyl)-3-aminopropyl-triethoxysilane) co-condensed mesoporous silica with a film

thickness around 115 nm and b) two layers consisting of a first mesoporous silica layer containing 5 mol% co-condensed (Bis(2-hydroxyethyl)-3-aminopropyl-triethoxysilane) and a second mesoporous silica layer resulting in around 220 nm film thickness. No clear interface between the two layers can be identified indicating a very homogenous structure. The samples were sputtered with Pt/Pd before measuring with SEM.

XPS results:

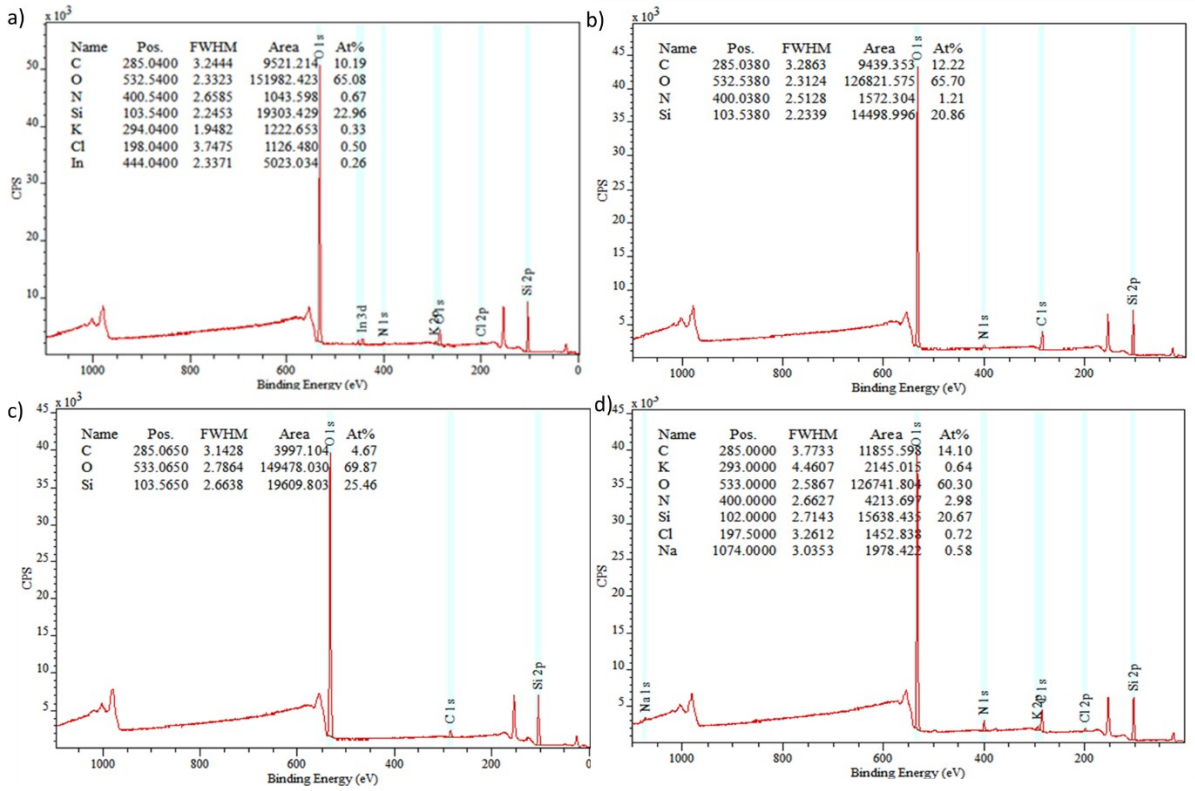

Figure S12. XP survey spectra of the double layered gravure printed mesoporous silica films. a) 1. 5 mol% co-condensed mesoporous silica 2. mesoporous silica b) 1. mesoporous silica 2.) 5 mol% co-condensed mesoporous silica c) two layers of mesoporous silica and d) two layers of 5 mol% co-condensed mesoporous silica. The mesoporous silica is co-condensed with (Bis(2-hydroxyethyl)-3-aminopropyl-triethoxysilane).

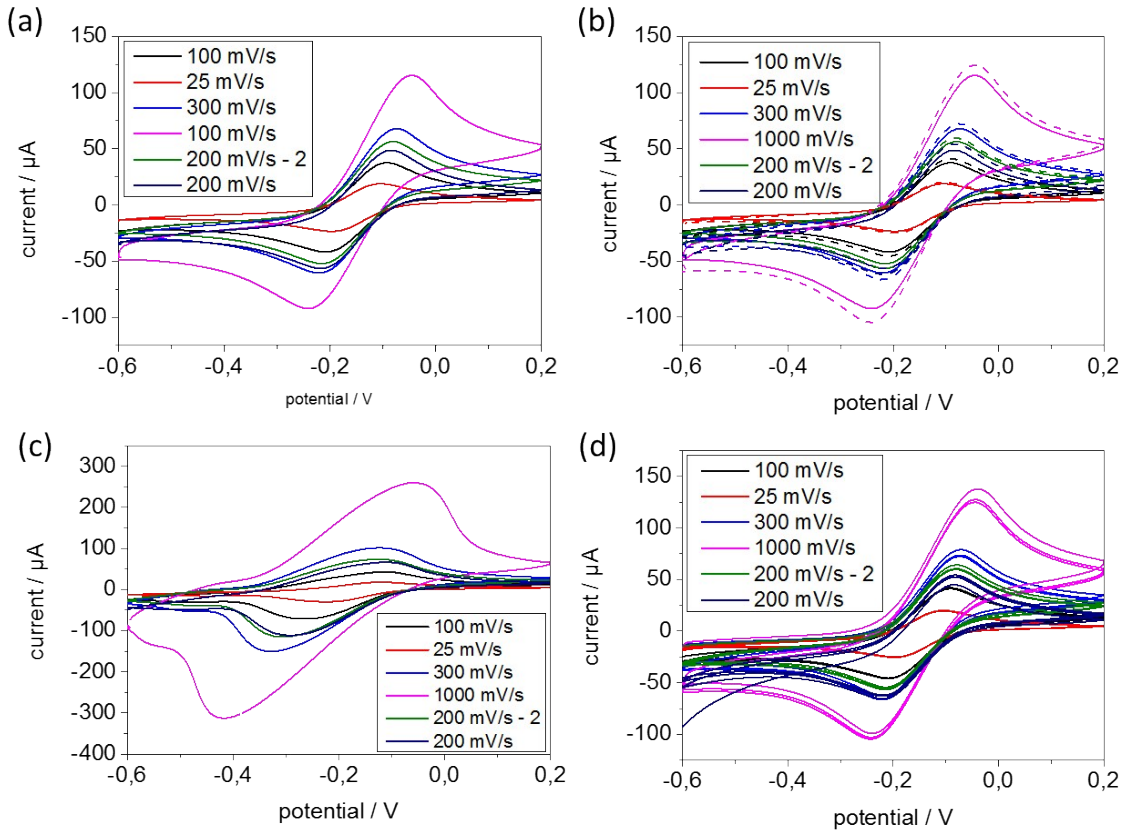

Figure S13. Exemplified qualitiy control in cyclic voltammetry measurements of mesoporous silica dip-coated with 2 mm/s withdrawal speed on ITO coated glass substrates. The measurements were performed with 1mmol $[Ru(NH_3)_6]^{2+/3+}$ dissolved in 0.1 M KCl at pH 3. a) Showing the different scan rates. The scanrate 200 mV/s is measured twice at the beginning and at the end after cycling all scan rates three times. Both cyclic voltammograms at this scan rate are very comparable and CV data is only discussed if this is the case. b) Showing the cyclic voltammograms for all measured scanrates at pH 3 before (line) and after (dashed line) measuring the same scanrates at pH 9. The obtained CV before and after measuring pH 9 are comparable and CV data is only discussed if this is the case. c) Showing the different scan rates including 200 mV/s as first and last scan in basic conditions at pH 9. d) Showing all three cycles measured for each scan rate. Usually the third cycle is shown after validating that the three cycles are comparable.

Ellipsometry results and calculation of porosity:

The Brüggemann effective medium approximation was used to calculate the volume porosity from the fitted refractive index of the mesoporous silica films.[4, 5] Therefore the following relationship between the dielectric constants and volume fraction of each constituent material exists:

$$V_{pore}\left(\frac{\varepsilon_{pore}-\varepsilon_{mesopSilica}}{\varepsilon_{pore}+2\varepsilon_{mesopSilica}}\right)+V_{silica}\left(\frac{\varepsilon_{silica}-\varepsilon_{mesopSilica}}{\varepsilon_{silica}+2\varepsilon_{mesopSilica}}\right)=0$$

where V_{pore} and V_{silica} correspond to the volume fractions occupied by air and silica, and ε_{pore}, ε_{silica} and $\varepsilon_{mesopSilica}$ correspond to the dielectric constants of air, silica, and the mesoporous

silica. Furthermore, the relations $V_{silica}+V_{pore}=1$ and $\varepsilon = n^2$ ($n_{air}=1$ and $n_{silica}=1.46$)[6] is valid so it is possible to gain the following formula and the pore volume/porousity can be calculated.

$$V_{pore}\left(\frac{1-n_{mesopSilica}^{2}}{1+2n_{mesopSilica}^{2}}\right)+(1-V_{pore})\left(\frac{2.1316-n_{mesopSilica}^{2}}{2.1316+2n_{mesopSilica}^{2}}\right)=0$$

Table S1. Ellipsometry results of printed mesoporous silica films with different cylinders of different cell volumes (mL/m^2). Values for film thickness and refractive index are obtained by fitting the obtained data to a one-box model. V_{pore} values are calculated using the Brüggemann approximation[7]. All samples printed on silicon wafer. Given errors are determined by standard deviation of minimal three measured points. Further experimental details are given within the experimental section.

Printing cell volume [mL m^{-2}]	Layer thickness [nm]	Refractive index	RMSE	V_{pore}* [vol%]
24	248.2 ± 8.6	1.262 ± 0.034	0.403	42
16.3	161.9 ± 4.9	1.270 ± 0.011	0.220	40
8.5	99.3 ± 2.3	1.231 ± 0.008	0.524	48
4.5	60.3 ± 2.0	1.272 ± 0.025	0.286	40

Table S2. Ellipsometry results of printed mesoporous silica films with different cylinders of different cell volumes (mL/m^2) for 6-8 nm pores. Values for film thickness and refractive index are obtained by fitting the obtained data to a one-box model. V_{pore} values are calculated using the Brüggemann approximation[7]. All samples printed on silicon wafer. Given errors are determined by standard deviation of minimal three measured points. Further experimental details are given within the experimental section.

Printing cell volume [mL m^{-2}]	Layer thickness [nm]	Refractive index	RMSE	V_{pore}* [vol%]
12.23	111.4 ± 2.1	1.319 ± 0.026	0.432	30
10.14	103.1 ± 0.9	1.249 ± 0.009	0.215	44
9.19	98.7 ± 2.3	1.287 ± 0.038	0.491	36
8.30	93.3 ± 0.8	1.253 ± 0.006	0.275	44
5.98	77.1 ± 2.0	1.255 ± 0.112	0.127	43
4.71	72.6 ± 4.7	1.271 ± 0.031	0.382	40
2.72	48.9 ± 0.8	1.406 ± 0.020	0.252	-
1.67	37.8 ± 0.2	1.459 ± 0.013	0.059	-
0.93	21.1 ± 0.6	1.500 ± 0.052	0.148	-
0.45	8.9 ± 1.6	1.872 ± 0.154	0.041	-

Table S3. Ellipsometry results of dip-coated mesoporous silica films with different withdrawal speeds (mm/s) for 6-8 nm pores. Values for film thickness and refractive index are obtained by fitting the obtained data to a one-box model. V_{pore} values are calculated using the Brüggemann approximation[7]. All samples printed on silicon wafer. Given errors are

determined by standard deviation of minimal three measured points. Further experimental details are given within the experimental section.

Withdrawal speed [mm s^{-1}]	Layer thickness [nm]	Refractive index	RMSE	V_{pore}* [vol%]
0.05	419.8 ± 127.6	1.210 ± 0.08	4.441	53
0.5	168.8 ± 14.4	1.235 ± 0.008	1.779	47
0.9	152.8 ± 16.3	1.252 ± 0.011	1.041	44
1	140.5 ± 6.8	1.242 ± 0.035	0.407	46
2	180.4 ± 7.5	1.250 ± 0.002	0.688	44
3	226.3 ± 5.0	1.253 ± 0.001	1.439	44
4	267.5 ± 2.9	1.259 ± 0.000	0.745	42
5	265.3 ± 2.5	1.261 ± 0.000	0.760	42
6	290.4 ± 3.4	1.273 ± 0.001	0.422	39
7	323.9 ± 16.5	1.265 ± 0.011	0.843	41
8	316.5 ± 0.7	1.278 ± 0.000	0.495	38
9	339.3 ± 11	1.299 ± 0.019	0.769	34
10	372.0 ± 13.2	1.275 ± 0.035	1.278	39
15	395.5 ± 34.2	1.245 ± 0.001	1.576	45
20	398.2 ± 46.6	1.270 ± 0.054	2.987	40
25	357.9 ± 8.4	1.282 ± 0.010	0.927	38
30	353.4 ± 4.7	1.269 ± 0.001	0.868	40

Table S4. Ellipsometry results of dip-coated mesoporous silica films with different withdrawal speeds (mm/s) for 8-16 nm pores. Values for film thickness and refractive index are obtained by fitting the obtained data to a one-box model. V_{pore} values are calculated using the Brüggemann approximation[7]. All samples printed on silicon wafer. Given errors are determined by standard deviation of minimal three measured points. Further experimental details are given within the experimental section.

Withdrawal speed [mm s^{-1}]	Layer thickness [nm]	Refractive index	RMSE	V_{pore}* [vol%]
0.25	256.9 ± 0.9	1.191 ± 0.001	0.706	57
0.5	292.0 ± 9.4	1.305 ± 0.029	2.215	33
1	318.6 ± 1.6	1.232 ± 0.004	0.377	48
1.5	530.9 ± 2.4	1.139 ± 0.002	0.937	68
2	595.5 ± 5.4	1.162 ± 0.005	2.614	63
4	906.7 ± 16	1.127 ± 0.008	3.433	70
7	856.7 ± 18	1.149 ± 0.011	3.778	66
10	1016 ± 17	1.149 ± 0.008	5.482	66

Table S5. Ellipsometry results of printed mesoporous silica films with different cylinders of different cell volumes (mL/m^2) for 8-16 nm. Values for film thickness and refractive index are obtained by fitting the obtained data to a one-box model. V_{pore} values are calculated using the Brüggemann approximation[7]. All samples printed on silicon wafer. Given errors are determined by standard deviation of minimal three measured points. Further experimental details are given within the experimental section.

Printing cell volume [mL m^{-2}]	Layer thickness [nm]	Refractive index	RMSE	V_{pore}* [vol%]

12.23	199.3 ± 3.3	1.220 ± 0.002	0.597	51
10.14	174.7 ± 4.1	1.222 ± 0.014	0.448	50
9.19	175.2 ± 2.8	1.217 ± 0.004	0.683	51
8.30	165.8 ± 3.4	1.215 ± 0.006	0.613	52
5.98	141.4 ± 1.4	1.214 ± 0.013	0.536	52
4.71	87.4 ± 0.6	1.212 ± 0.018	0.323	52
1.67	59.0 ± 1.2	1.239 ± 0.002	0.136	47
0.93	35.8 ± 1.8	1.346 ± 0.040	0.128	24
0.45	19.4 ± 1.0	1.378 ± 0.264	0.214	17

Table S6. Ellipsometry results of printed mesoporous silica films co-condensed with (Bis(2-hydroxyethyl)-3-aminopropyl-triethoxysilane). Values for film thickness and refractive index are obtained by fitting the obtained data to a one-box model. V_{pore} values are calculated using the Brüggemann approximation.[7] All samples printed on silicon wafer. Given errors are determined by standard deviation of minimal three measured points. Further experimental details are given within the experimental section.

Co-initiator [%]	Layer thickness [nm]	Refractive index	RMSE	V_{pore}^{*} [vol%]
0	99.3 ± 2.3	1.231 ± 0.008	0.524	48
Post-grafted	104.9 ± 4.7	1.282 ± 0.001	0.899	37
5 (co-condensed)	121.2 ± 2.3	1.253 ± 0.017	0.754	43
10 (co-condensed)	121.5 ± 3.5	1.230 ± 0.006	0.671	48
15 (co-condensed)	122.2 ± 0.6	1.238 ± 0.038	0.426	47
20 (co-condensed)	117.1 ± 1.8	1.240 ± 0.006	0.437	46

Table S7. Surface composition obtained by XPS analysis based on the results shown in Figure S**12**. Please note that not all compositions add up to 100% due to rounding.

rel. to Figure S10	sample	N	C	O	Si	K	Na	In	Cl
		at%	at%	at%	at%	at%	at%	at%	at%
a)	1. mesop. silica 5 mol% co-condensed 2. mesop. silica	0.7	10.2	65.1	23.0	0.3		0.3	0.5
b)	1. mesop. silica 2. mesop. silica 5 mol% co-condensed	1.2	12.2	65.7	20.9				
c)	1. mesop. silica 2. mesop. silica		4.7	69.9	25.5				
d)	1. mesop. silica 5 mol% co-condensed 2. mesop. silica 5 mol% co-condensed	2.9	14.1	60.3	20.7	0.6	0.6		0.7

References

1. M. Faustini, D. R. Ceratti, B. Louis, M. Boudot, P. A. Albouy, C. Boissiere and D. Grosso, *ACS Appl Mater Interfaces*, 2014, **6**, 17102-17110.
2. M. Sulpizi, M. P. Gaigeot and M. Sprik, *J Chem Theory Comput*, 2012, **8**, 1037-1047.

3. J. M. Rosenholm, T. Czuryszkiewicz, F. Kleitz, J. B. Rosenholm and M. Lindén, *Langmuir*, 2007, **23**, 4315-4323.
4. J. Tom, R. Brilmayer, J. Schmidt and A. Andrieu-Brunsen, *Polymers*, 2017, **9**, 539.
5. A. Brunsen, A. Calvo, F. J. Williams, G. J. Soler-Illia and O. Azzaroni, *Langmuir*, 2011, **27**, 4328-4333.
6. I. H. Malitson, *Journal of the Optical Society of America*, 1965, **55**, 1205-1209.
7. J. E. Spanier and I. P. Herman, *Physical Review B*, 2000, **61**, 10437-10450.